Realistic shell-model calculations for isotopic chains "north-east" of ^{48}Ca in the (N,Z) plane

L. Coraggio,[1] A. Covello,[2] A. Gargano,[1] and N. Itaco[1,2]

[1]*Istituto Nazionale di Fisica Nucleare, Complesso Universitario di Monte S. Angelo, Via Cintia - I-80126 Napoli, Italy*

[2]*Dipartimento di Fisica, Università di Napoli Federico II, Complesso Universitario di Monte S. Angelo, Via Cintia - I-80126 Napoli, Italy*

(Received 16 October 2013; revised manuscript received 9 December 2013; published 26 February 2014)

We perform realistic shell-model calculations for nuclei with valence nucleons outside ^{48}Ca, employing two different model spaces. The matrix elements of the effective two-body interaction and electromagnetic multipole operators have been calculated within the framework of many-body perturbation theory, starting from a low-momentum potential derived from the high-precision CD-Bonn free nucleon-nucleon potential. The role played by the neutron orbital $1d_{5/2}$ has been investigated by comparing experimental data on yrast quadrupole excitations of isotopic chains north-east of ^{48}Ca with the results of calculations including or not including this single-particle state in the model space.

DOI: 10.1103/PhysRevC.89.024319 PACS number(s): 21.60.Cs, 23.20.Lv, 27.40.+z, 27.50.+e

I. INTRODUCTION

An interesting aspect of the physics of nuclei approaching the neutron drip line is the evolution of their shell structure. This topic is currently investigated in different mass regions, and the modern advances in the detection techniques and new experimental devices provide data that drive to a better understanding of the microscopic mechanism underlying modifications of the "magic numbers."

In this context, in the last decade the key role played by the tensor component of the residual two-body interaction between spin-orbit partner single-particle states has been recognized [1–3]. This may give rise to a breaking of shell closures leading to the possible appearance of the so-called "island of inversion;" namely, a region of nuclei where a rapid development of collectivity is observed. The best-known example of this phenomenon is given by neutron-rich nuclei around ^{32}Mg [4].

The region of nuclei with valence protons outside doubly closed ^{48}Ca may be considered an interesting laboratory to study the shell evolution when adding neutrons, since there are long isotopic chains, such as those of iron and nickel isotopes, whose exoticity reaches an N/Z value of 1.79 in ^{78}Ni.

As a matter of fact, it can be observed that the shell closure at $N = 40$ in ^{68}Ni, corresponding to the filling of the neutron fp orbitals and of the proton $f_{7/2}$ orbital, rapidly disappears when removing protons from $f_{7/2}$, as testified by the behavior of the experimental excitation energies of the yrast $J^\pi = 2^+$ states in iron and chromium neutron-rich isotopes.

For these isotopic chains several experimental studies (see, for example, Refs. [5–9]) have found out that the disappearance of the $N = 40$ shell closure comes along with the onset of collective behavior, as indicated for instance by the observation of a rapid increase of the ratio $E_x(4_1^+)/E_x(2_1^+)$ in $^{60-64}$Cr [10,11]. This has been related to the correlations between the quadrupole-partner neutron orbitals $0g_{9/2}$ and $1d_{5/2}$ [12–14], so, within a shell-model description of these nuclei, the inclusion of the neutron $1d_{5/2}$ orbital should be needed.

It is worth pointing out that there is a general belief [15] that shell-model effective interactions derived from realistic nucleon-nucleon (NN) potentials are defective in their monopole component, so that they are not able to provide a good description of the evolution of spectroscopic properties along the isotopic chains, unless including contributions from three-nucleon forces [16,17].

On these grounds, we have found it challenging to perform realistic shell-model calculations [18] for some isotopic chains north-east of ^{48}Ca, starting from the high-precision CD-Bonn NN potential renormalized by way of the so-called $V_{\text{low-k}}$ approach [19,20]. In particular, in order to explore the microscopic processes leading to the disappearance of the $N = 40$ shell closure and the onset of collectivity, we have derived two effective shell-model interactions for two different model spaces. The first one, which is spanned by the proton $0f_{7/2}$ and $1p_{3/2}$ orbitals and by the neutron $1p_{3/2}$, $1p_{1/2}$, $0f_{5/2}$, $0g_{9/2}$ orbitals, is able, as we show in the following, to reproduce the dropping of the $N = 40$ magic number in iron and chromium isotopes as well as many other spectroscopic properties of nuclei north-east of ^{48}Ca. The second one is spanned by the same orbitals plus the neutron $1d_{5/2}$. The calculations within the latter model space are able to reproduce the onset of collectivity in heavy iron and chromium isotopes, at the same time preserving the results obtained with the first model space.

In the following section, we outline the perturbative approach to the derivation of our shell-model Hamiltonians and effective charges of the electric quadrupole operators. In Sec. III, we present the results of our calculations for calcium, titanium, chromium, iron, and nickel isotopes. Concluding remarks are given in the last section. In the Appendix, we report the calculated two-body matrix elements (TBME) of the effective shell-model interactions, the employed single-particle (SP) energies, and the effective charges of the $E2$ operator.

II. OUTLINE OF CALCULATIONS

Within the framework of the shell model, an auxiliary one-body potential U is introduced in order to break up the

Hamiltonian for a system of A nucleons as the sum of a one-body term H_0, which describes the independent motion of the nucleons, and a residual interaction H_1:

$$H = \sum_{i=1}^{A} \frac{p_i^2}{2m} + \sum_{i<j=1}^{A} V_{ij}^{NN} = T + V = (T + U) + (V - U) = H_0 + H_1. \quad (1)$$

Once H_0 has been introduced, it is possible to define a reduced model space in terms of a finite subset of H_0's eigenvectors. In this space, an effective Hamiltonian $H_{\rm eff}$ may be constructed and the diagonalization of the many-body Hamiltonian (1) in an infinite Hilbert space is then reduced to the solution of an eigenvalue problem in a finite space.

As mentioned in the Introduction, we derive effective shell-model Hamiltonians $H_{\rm eff}$ for two model spaces outside the ^{48}Ca core. The first one (I) is spanned by the two single-proton levels $0f_{7/2}$, $1p_{3/2}$ and the four single-neutron levels $1p_{3/2}, 1p_{1/2}$, $0f_{5/2}, 0g_{9/2}$, while the second one (II) includes also the neutron $1d_{5/2}$ orbital.

To this end, the following approach has been employed: first we derived an $H_{\rm eff}$ defined in a very large model space outside the ^{40}Ca closed core and spanned by six proton and neutron $pfgd$ orbitals. Then, we derive from this $H_{\rm eff}$ two new effective Hamiltonians, defined in the smaller model spaces (I) and (II). The above double-step procedure ensures that, when the $1d_{5/2}$ orbital is irrelevant to describe the physics of certain nuclear states, the eigenvalues obtained using model space (I) or (II) are the same or at least very close to each other.

The derivation of both $H_{\rm eff}$s has been done in the framework of the time-dependent perturbation theory by way of the Kuo–Lee–Ratcliff (KLR) folded-diagram expansion [21]. More precisely, we first renormalize the high-momentum repulsive components of the CD-Bonn NN potential by way of the $V_{\rm low\text{-}k}$ approach [19,20] with a momentum cutoff $\Lambda = 2.6$ fm^{-1}, which provides a smooth potential preserving exactly the on-shell properties of the original NN potential. Next, we express $H_{\rm eff}$ in terms of the vertex function $\hat{Q}$-box, which is composed of irreducible valence-linked diagrams [22,23]. In the derivation of the $\hat{Q}$-box we have included one- and two-body Goldstone diagrams through third order in H_1 [24]. Since calculations beyond the third order in perturbation theory are computationally prohibitive, we have calculated the Padé approximant [2|1] [25,26] of the $\hat{Q}$-box, so as to obtain a value to which the perturbation series should converge, as suggested in Ref. [27]. The folded-diagram series is then summed up to all orders using the Lee–Suzuki iteration method [28].

The Hamiltonian $H_{\rm eff}$ contains one-body contributions, whose collection is the so-called $\hat{S}$-box [29]. In realistic shell-model calculations a subtraction procedure is commonly used, so as to retain only the TBME of $H_{\rm eff}$ ($V_{\rm eff}$), while the SP energies are taken from experiment. This approach enables to take into account implicitly the effects of three-body forces on the SP energies.

In this work, the proton SP energy spacing is taken from the experimental one between the yrast $\frac{3}{2}^-$ state and the $\frac{7}{2}^-$ ground state in ^{49}Sc [30], which are mainly of single-particle nature [31], so that $\epsilon_{p_{3/2}} - \epsilon_{f_{7/2}} = 3.1$ MeV. Similarly, the two neutron $\epsilon_{p_{1/2}} - \epsilon_{p_{3/2}}$, $\epsilon_{f_{5/2}} - \epsilon_{p_{3/2}}$ spacings are taken from the experimental spectrum of ^{49}Ca, considering the yrast $\frac{1}{2}^-$ and the yrare $\frac{5}{2}^-$ states [30], that have the largest observed single-particle components [32]. As regards the neutron $0g_{9/2}$ state, at present there is no experimental indication of the existence of such a state in ^{49}Ca, therefore we have fixed its energy so as to reproduce the experimental odd-even mass difference around ^{68}Ni [33]. All the observed $\frac{5}{2}^+$ states in ^{49}Ca do not exhibit a significant SP component, so we have chosen a value of the $1d_{5/2}$ energy which gives, when using model space (II), an odd-even mass difference around ^{80}Zn in a reasonable agreement with the estimated value [33]. In summary, our adopted neutron SP energy spacings for model space (I) are $\epsilon_{p_{1/2}} - \epsilon_{p_{3/2}} = 2.0$ MeV, $\epsilon_{f_{5/2}} - \epsilon_{p_{3/2}} = 4.0$ MeV, $\epsilon_{g_{9/2}} - \epsilon_{p_{3/2}} = 4.1$ MeV, and for model space (II) $\epsilon_{g_{9/2}} - \epsilon_{p_{3/2}} = 3.8$ MeV and $\epsilon_{d_{5/2}} - \epsilon_{p_{3/2}} = 8.0$ MeV.

The SP energies and TBME relative to ^{48}Ca used in the present calculation can be found in Tables I, II, III, and IV while the proton and neutron effective charges of the electric quadrupole operator, that have been derived consistently with $H_{\rm eff}$, are in Tables V and VI. It should be pointed out that for protons the Coulomb force has been explicitly added to $V_{\rm low\text{-}k}$ before constructing $V_{\rm eff}$.

III. RESULTS

In this section, we report the results of our shell-model calculations for calcium, titanium, chromium, iron, and nickel isotopes with mass number $A > 48$ and compare them with the available experimental data. As mentioned in the Introduction, our attention is focused on the insurgence of collective behavior or shell-closure properties when adding valence neutrons.

The calculations have been performed by using the OSLO shell-model code [34].

A. Calcium isotopes

A major topic in nuclear physics is the understanding of the shell evolution towards the neutron dripline, and in this context the study of calcium isotopes provides an interesting laboratory [17,35–38].

An extensive study of the heavy calcium isotopes has been reported in Ref. [39], where we have performed a shell-model calculation using ^{40}Ca as an inert core and the full fp shell as model space. As in the present paper, the effective interaction has been obtained from a $V_{\rm low\text{-}k}$ derived from the CD-Bonn potential with a cutoff momentum equal to 2.6 fm^{-1}. The results we obtained are in excellent agreement with the experimental data, in particular we successfully predicted the excitation energy of the yrast $J = 2^+$ in ^{54}Ca, that only recently has been measured at RIKEN [40].

Figure 1 reports the excitation energies of the yrast 2^+ states calculated with model spaces (I) and (II) as a function

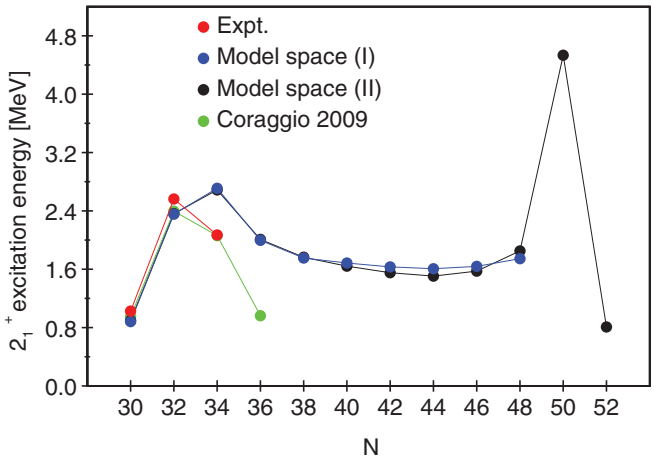

FIG. 1. (Color online) Experimental [30,40] and calculated excitation energies of the yrast $J^\pi = 2^+$ states for calcium isotopes.

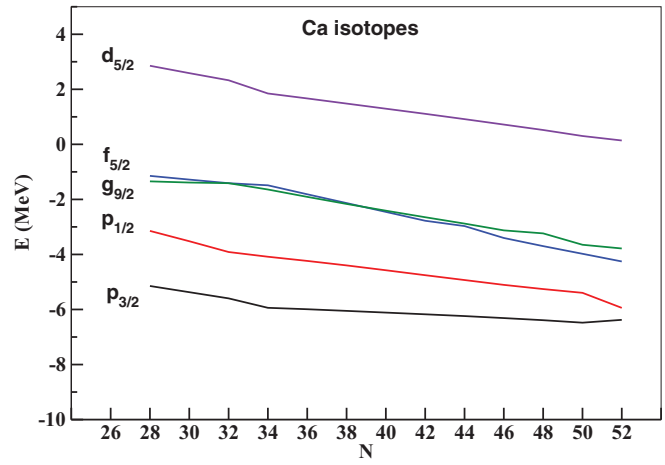

FIG. 2. (Color online) Calculated neutron effective single-particle energies for calcium isotopes from $N = 30$ to 52.

of the neutron number up to $N = 52$ and compared with the available experimental data and the results obtained by our previous calculations with the full fp-shell-model space.

It can be seen that the available observed energies are well reproduced for $N = 30,32$; the three calculations providing almost the same values. At $N = 34,36$ the results with model spaces (I) and (II) differ from those of Ref. [39] and are almost indistinguishable up to $N = 48$. We have verified that to reproduce the observed drop in energy at $N = 34$ it is necessary, as in Ref. [39], to include explicitly the neutron $0f_{7/2}$ orbital into the model space. On the other hand, the different results obtained at $N = 36$ trace back to the presence in model spaces (I) and (II) of the $0g_{9/2}$ orbital that starts to fill just at $N = 36$. As a matter of fact, we have verified that, when blocking out this orbital, the calculated excitation energy of the yrast 2^+ state drops abruptly down at 0.7 MeV.

This suggests that to optimize the description of the calcium isotopic chain one has to adopt a model space spanned by the full fp shell plus the $0g_{9/2}$ orbital.

From the inspection of Fig. 1, it can be seen that no shell closure shows up at $N = 40$, since the $0g_{9/2}$ SP energy is very close to the pf ones, while the large energy gap between $0g_{9/2}$ and $1d_{5/2}$ orbitals is responsible for a strong shell closure at $N = 50$ and that, according to our calculations, ^{70}Ca should be the last bound calcium isotope. This picture is confirmed when looking at the behavior of the calcium effective single-particle energies (ESPEs), as reported in Fig. 2.

B. Titanium isotopes

The calculated excitation energies of the yrast 2^+ states and the $B(E2; 2_1^+ \to 0_1^+)$ transition rates for titanium isotopes are reported in Fig. 3 up to $N = 40$. It can be seen that the observed excitation energies and $B(E2)$s are well reproduced by both calculations.

The decrease of the experimental 2_1^+ excitation energy in ^{56}Ti is linked to the lack of a $N = 34$ shell closure, as we predicted in Ref. [39] and confirmed by the recent observation of the excitation energy of $J^\pi = 2_1^+$ state in ^{54}Ca [40].

From inspection of Fig. 3, it can be observed that the calculated 2_1^+ excitation energies are almost insensitive to the inclusion of the $1d_{5/2}$ orbital. This does not happen with the $B(E2)$s, whose calculated values begin to differ substantially starting from $N = 36$ on. In particular, using model space (I) the increase of the number of valence neutrons corresponds to a rise of the proton $0f_{7/2}$ occupation number and to the decrease of the proton polarization, at variance with model space (II) where the occupation of this orbital is almost constant respect to the neutron number N (see Table VII). This comes with a significantly larger occupation of the neutron

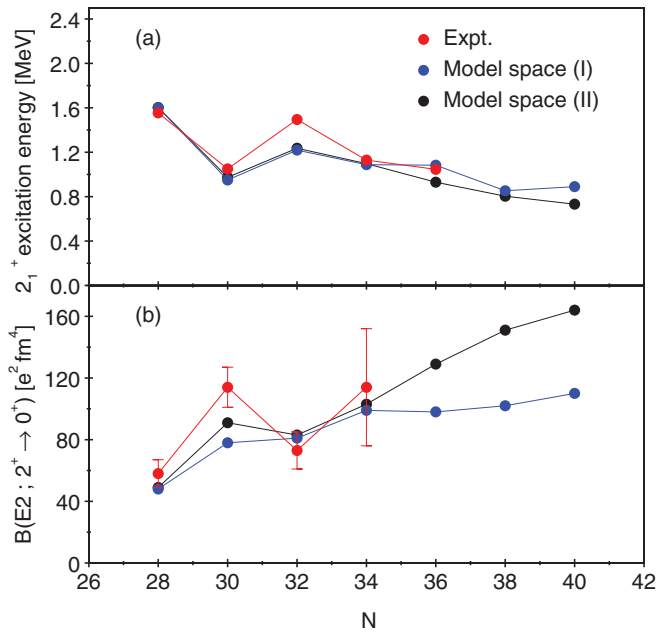

FIG. 3. (Color online) (a) Experimental [30,48] and calculated excitation energies of the yrast $J^\pi = 2^+$ states and (b) $B(E2; 2_1^+ \to 0_1^+)$ transition rates for titanium isotopes.

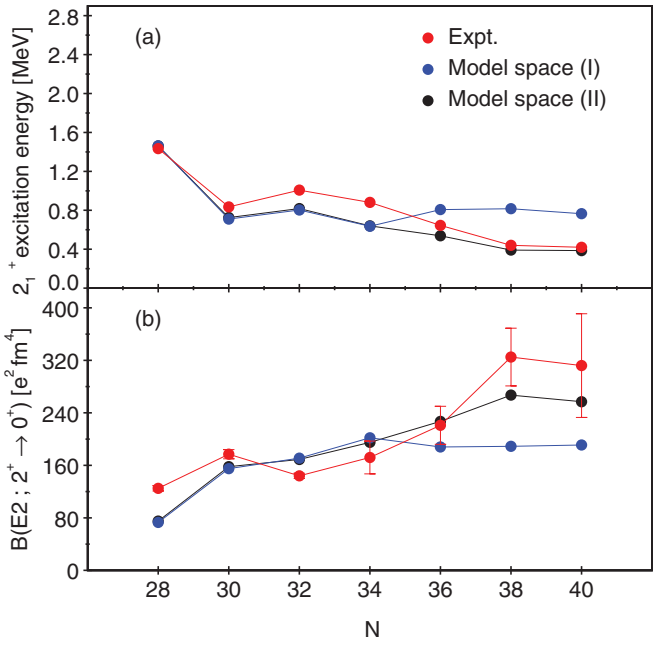

FIG. 4. (Color online) Same as in Fig. 3, but for chromium isotopes. Experimental data are taken from [30,49].

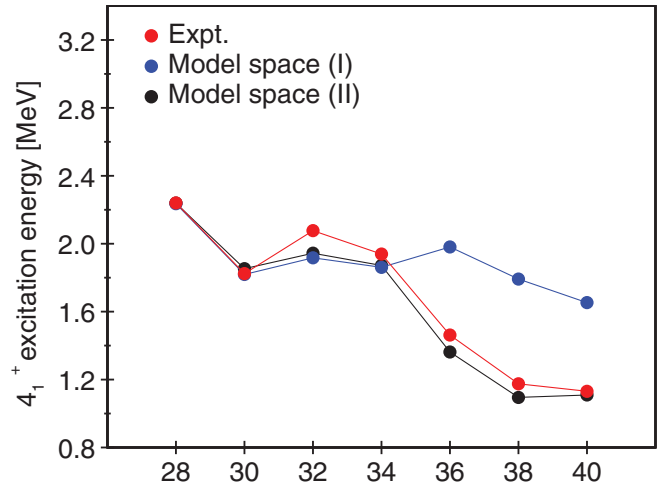

FIG. 5. (Color online) Experimental [30] and calculated excitation energies of the yrast $J^\pi = 4^+$ for Cr isotopes. See text for details.

$0g_{9/2}$ orbital with model space (II) with respect to model space (I), as well as an increase of the neutron $1d_{5/2}$-orbital occupation that provides a constant rise of the corresponding $B(E2)$s up to $N = 40$.

C. Chromium isotopes

The excitation energies of the yrast 2^+ states and $B(E2; 2_1^+ \rightarrow 0_1^+)$ transition rates for the chromium isotopes are reported in Fig. 4 up to $N = 40$. It is worth mentioning that the observed lowering of the yrast 2^+ states starting from $N = 34$ is interpreted as a signature of the development of a pronounced collectivity towards $N = 40$ [11]. The interpretation of such a collective behavior may be framed within the quasi-SU(3) approximate symmetry owing to the interplay between the quadrupole-quadrupole component of the residual interaction and the central field in the subspace spanned by the lowest $\Delta j = 2$ orbitals of a major shell [12]. In this connection, the need to include the neutron $1d_{5/2}$ orbital in a shell-model calculation, in order to produce the onset of collectivity around $N = 40$ in chromium isotopes, has been evidenced by Caurier, Nowacki, and Poves in Ref. [13].

Our results also support the crucial role played by this orbital. In fact, from inspection of Fig. 4 it can be observed that using model space (I) from ^{58}Cr to ^{60}Cr the calculated $J^\pi = 2_1^+$ states start to rise in excitation energy, while the experimental behavior does the opposite. Actually, by employing the model space (II), there is a decrease of the 2^+ excitation energy from $N = 34$ to $N = 36$. From the inspection of Table VII, we see that the appearance of the differences between the model-space (I) and (II) results come together with an abrupt increase of the occupation number of the neutron $1d_{5/2}$,$0g_{9/2}$ orbitals and a depletion of the proton $0f_{7/2}$ one. This has to be ascribed to a reduced neutron gap between $0g_{9/2} - 0f_{5/2}$ (about 2.5 MeV) effective single-particle energies (ESPEs) with respect to the one in Ni isotopes (about 4.0 MeV), where a shell closure is found at $N = 40$ (see Sec. IV), as well as to the quadrupole-quadrupole component of the effective interaction between the $1d_{5/2}$ and the $0g_{9/2}$ orbitals.

Another feature that reveals the onset of the collectivity in chromium isotopes is the rise of the experimental $B(E2; 2_1^+ \rightarrow 0_1^+)$ transition rates from $N = 34$ to $N = 38$. This can be reproduced only by calculations with model space (II), as can be seen in Fig. 4, where the experimental data are compared with our shell-model results with both model spaces.

In Fig. 5 the calculated and experimental excitation energies of the yrast 4^+ states are also reported, evidencing that only with model space (II) it is possible to reproduce the observed increase of the ratio $E_x(4_1^+)/E_x(2_1^+)$ from ^{60}Cr to ^{62}Cr.

D. Iron isotopes

In Fig. 6 the 2_1^+ excitation energies and $B(E2; 2_1^+ \rightarrow 0_1^+)$ transition rates of even iron isotopes are shown as a function of the neutron number up to $N = 40$. It should be mentioned that experimental data are available for ^{68}Fe too [41], but they are not reported since for this nucleus calculations performed with model space (II) need a CPU time which exceeds our present computational resources.

A relevant feature that can be inferred from Fig. 6 is the abrupt enhancement of $B(E2; 2_1^+ \rightarrow 0_1^+)$ in ^{64}Fe [7,8,41] that, as in chromium isotopes, is the evidence of the onset of a quadrupole collectivity. This is at variance with the results of calculations with model space (I), which show a decrease of $B(E2; 2_1^+ \rightarrow 0_1^+)$ from ^{62}Fe to ^{64}Fe. Actually, the onset of the above-mentioned quadrupole collectivity is reproduced using model space (II), and, as in Ti and Cr

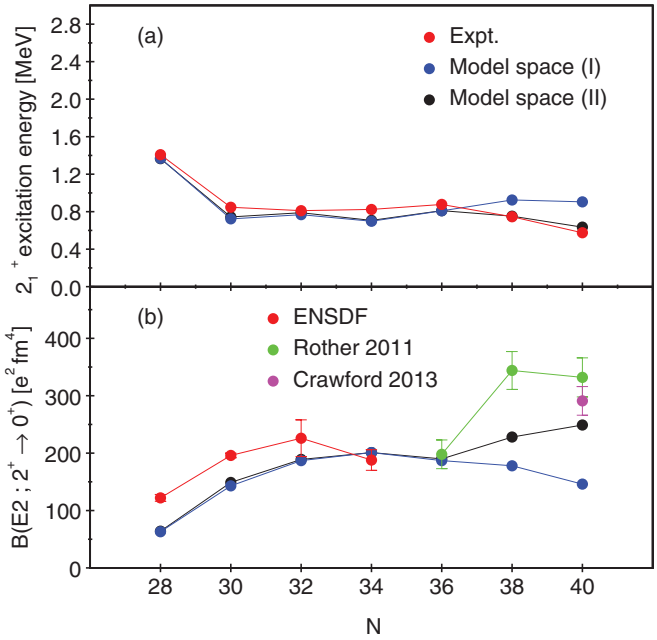

FIG. 6. (Color online) Same as in Fig. 3, but for iron isotopes. Experimental data are taken from ENSDF [30], Rother 2011 [8], and Crawford 2013 [41].

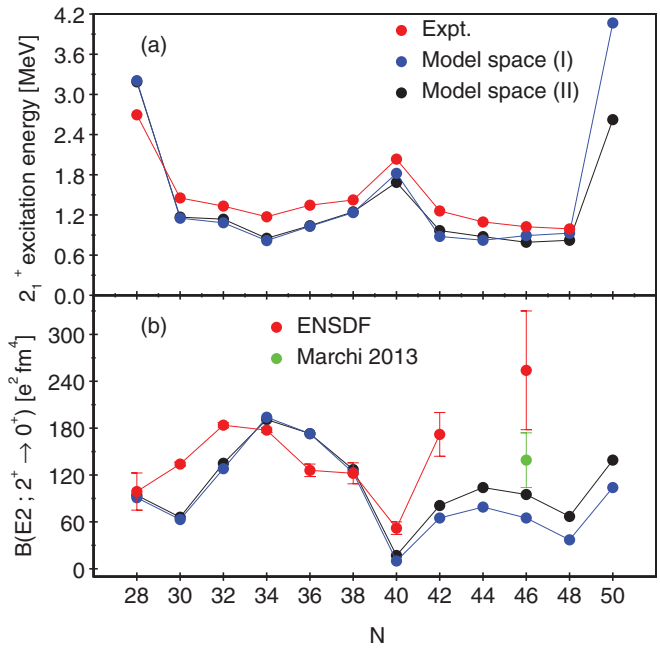

FIG. 7. (Color online) Same as in Fig. 3, but for nickel isotopes. Experimental data are taken from ENSDF [30] and Marchi 2013 [43].

isotopes, comes with a rise of the occupation number of the neutron $0g_{9/2}$ orbital (see Table VII). It has to be pointed out, however, that the experimental datum in ^{64}Fe [8] is underestimated.

E. Nickel isotopes

The nickel isotopes represent a very interesting laboratory to study the effects of the NN interaction on the shell evolution, when increasing the number of valence neutrons. In fact, this is a very long isotopic chain with available spectroscopic data from $N = 24$ up to $N = 48$, and several efforts are at present devoted to get as much experimental information as possible on ^{78}Ni, which is a possible waiting point for r-process nucleosynthesis [42]. Figure 7 reports the experimental data and the results of our shell-model calculations with model spaces (I) and (II) for the 2_1^+ excitation energy and the $B(E2; 2_1^+ \rightarrow 0_1^+)$ systematics from $N = 28$ to $N = 50$.

As already mentioned in the Introduction, it can be seen that the filling of the proton $0f_{7/2}$ orbital, corresponding to the well-known $Z = 28$ closure, produces the disappearance of the collectivity towards $N = 40$ observed in chromium and iron isotopes. The peak of the yrast 2^+ excitation energy and the fall of the corresponding $B(E2)$ in ^{68}Ni is a clear manifestation of the shell closure at $N = 40$, which is added to the ones at $N = 28$ and $N = 50$ in this long isotopic chain. As a matter of fact, it turns out that our calculated neutron ESPEs provide a large gap between the $0g_{9/2}$ and fp orbitals (see Fig. 8).

This implies a minor role played by the correlations between the quadrupole partners $0g_{9/2}, 1d_{5/2}$, as supported by the fact that the calculations with model space (I) and (II) give similar occupation numbers (see Table VII), as well as the same behavior for the $E_x(2_1^+)$ and the electric-quadrupole transition rates (see Fig. 7).

It is interesting to note that recently the $B(E2; 2_1^+ \rightarrow 0_1^+)$ in ^{74}Ni has been measured in a Coulomb excitation experiment [43], the obtained value being significantly smaller than the one measured indirectly via a (p, p') inelastic diffusion [44]. Our values of the $B(E2)$s for ^{74}Ni are close to the recently measured one. They, however, do not reproduce the decrease in $B(E2)$ from $N = 42$ to $N = 46$ since the ^{70}Ni $B(E2)$ is significantly underestimated. More precisely, we predict an increase of $B(E2)$ from $N = 40$ to 42 but not as large as the observed one. This may be traced to the fact that our proton

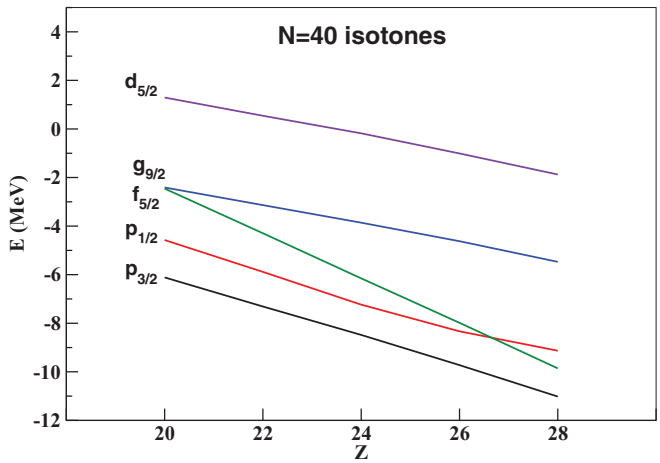

FIG. 8. (Color online) Calculated neutron effective single-particle energies for Ti, Cr, Fe, and Ni isotopes at $N = 40$.

model space leaves out the $0f_{5/2}$ orbital, which has a relevant role beyond $N = 40$ as evidenced by the behavior of the yrast $\frac{5}{2}^-$ states in odd-mass Cu isotopes [30]. As a matter of fact, for Ni isotopes with $N > 40$ the attraction due to the tensor force between the neutron $0g_{9/2}$ and the proton $0f_{5/2}$ orbitals may give rise to a lowering of the latter leading to a strong core polarization with a consequent increase of the $B(E2)$s. It is worth mentioning, however, that shell-model calculations that include explicitly the proton $0f_{5/2}$ orbital show the same behavior of $B(E2)$ as ours [45].

Finally, it has to be observed that, because of the magicity at $N = 50$, the yrast $J = 2^+$ state in ^{78}Ni is built up, breaking a couple of protons in the filled $0f_{7/2}$ orbital and promoting one proton into the $1p_{3/2}$ orbital. This mechanism is then responsible of the increase of the theoretical $B(E2; 2^+ \to 0^+)$ with respect to neighboring nuclei.

IV. CONCLUDING REMARKS

We have presented here the results of an extensive shell-model study of nuclei north-east of ^{48}Ca within the framework of a microscopic approach. This means that, starting from a $V_{\text{low-k}}$ derived from the CD-Bonn NN potential, effective two-body interactions and effective electromagnetic multipole operators have been calculated by way of perturbation theory and then employed in shell-model calculations.

As mentioned in the Introduction, this region is currently the subject of many experimental and theoretical investigations, especially because of the behavior of the quadrupole collectivity at $N = 40$ versus the atomic number, as can be inferred from the inspection of Fig. 9.

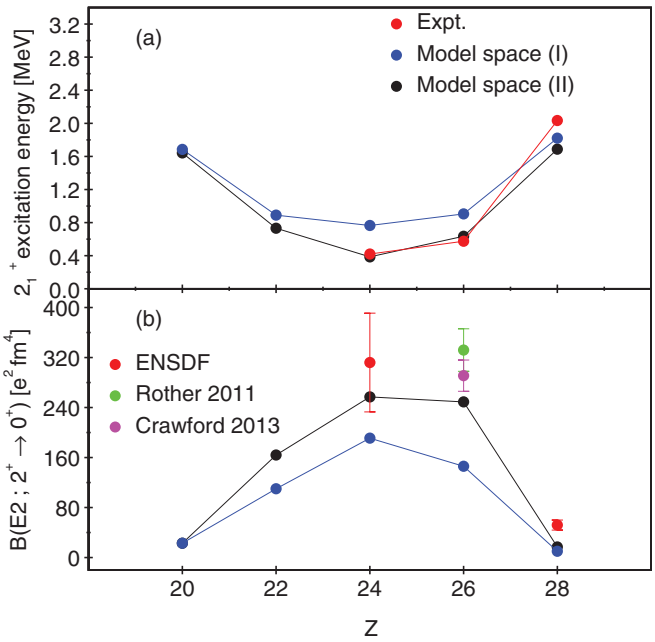

FIG. 9. (Color online) (a) Experimental (ENSDF: [30], Rother 2011: [8], Crawford 2013: [41]) and calculated excitation energies of the yrast $J^\pi = 2^+$ states and (b) $B(E2; 2_1^+ \to 0_1^+)$ transition rates for the $N = 40$ isotones.

In this context, we have focused attention on the role played by the neutron $1d_{5/2}$ orbital in the spectroscopy of the nuclei under investigation, using two different model spaces which differ only by the inclusion of this SP state.

Our results are in a better agreement with experiment when using the larger model space, in line with other large-scale shell-model calculations [14,45–47] where the TBMEs were determined empirically. This confirms the ability of realistic shell-model calculations to provide a reliable microscopic description of the shell evolution along isotopic chains, even in the presence of strong collective features. In fact, results with model spaces (I) and (II) are similar only for Ni isotopes, evidencing the relevance of including the neutron $1d_{5/2}$ orbital to describe the collective properties of Ti, Cr, and Fe isotopic chains. The role played by $1d_{5/2}$ may be explained in terms of correlations between this orbital and its quadrupole partner $0g_{9/2}$, which comes into play because of the reduction of the $0f_{5/2} - 0g_{9/2}$ gap.

The above considerations are clearly illustrated by the behaviour of the ESPEs, see Fig. 8, as well as by that of the energies of the yrast 2^+ states and of the $B(E2; 2_1^+ \to 0_1^+)$ transition rates, which are reported in Fig. 9 as functions of Z for $N = 40$. From the inspection of Fig. 9, it can be clearly seen that the nature of the yrast 2^+ states changes with the filling of the proton $0f_{7/2}$ orbital, tuning the collectivity at $N = 40$.

It has to be stressed that our calculations employ only a two-body $V_{\text{low-k}}$, derived from the high-precision CD-Bonn potential, not taking into account any three-body forces. Therefore, the good quality of the agreement between theory and experiment seems to question the role of valence three-body forces in the description of the spectroscopic properties of intermediate-mass nuclei.

APPENDIX

TABLE I. Shell-model proton single-particle energies (in MeV) employed in present work (see text for details). The value of the $\epsilon_{f_{7/2}}$ is taken from the one-proton separation energy of ^{49}Sc [33].

nlj	Model space (I) and (II)
$0f_{7/2}$	−9.627
$1p_{3/2}$	−6.527

TABLE II. Shell-model neutron single-particle energies (in MeV) employed in present work (see text for details). The value of the $\epsilon_{p_{3/2}}$ is taken from the one-neutron separation energy of ^{49}Ca [33].

nlj	Model space (I)	Model space (II)
$1p_{3/2}$	−5.157	−5.157
$1p_{1/2}$	−3.157	−3.157
$0f_{5/2}$	−1.157	−1.157
$0g_{9/2}$	−1.057	−1.357
$1d_{5/2}$		2.843

TABLE III. Proton-proton, neutron-neutron, and proton-neutron matrix elements (in MeV) derived for calculations in model space (I). They are antisymmetrized and normalized by a factor $1/\sqrt{(1+\delta_{j_a j_b})(1+\delta_{j_c j_d})}$.

$n_a l_a j_a$	$n_b l_b j_b$	$n_c l_c j_c$	$n_d l_d j_d$	J	T_z	TBME
$0f_{7/2}$	$0f_{7/2}$	$0f_{7/2}$	$0f_{7/2}$	0	1	−2.021
$0f_{7/2}$	$0f_{7/2}$	$1p_{3/2}$	$1p_{3/2}$	0	1	−1.219
$1p_{3/2}$	$1p_{3/2}$	$1p_{3/2}$	$1p_{3/2}$	0	1	−0.058
$0f_{7/2}$	$0f_{7/2}$	$0f_{7/2}$	$0f_{7/2}$	2	1	−0.414
$0f_{7/2}$	$0f_{7/2}$	$0f_{7/2}$	$1p_{3/2}$	2	1	−0.704
$0f_{7/2}$	$0f_{7/2}$	$1p_{3/2}$	$1p_{3/2}$	2	1	−0.355
$0f_{7/2}$	$1p_{3/2}$	$0f_{7/2}$	$1p_{3/2}$	2	1	−0.547
$0f_{7/2}$	$1p_{3/2}$	$1p_{3/2}$	$1p_{3/2}$	2	1	−0.356
$1p_{3/2}$	$1p_{3/2}$	$1p_{3/2}$	$1p_{3/2}$	2	1	0.108
$0f_{7/2}$	$1p_{3/2}$	$0f_{7/2}$	$1p_{3/2}$	3	1	0.329
$0f_{7/2}$	$0f_{7/2}$	$0f_{7/2}$	$0f_{7/2}$	4	1	0.133
$0f_{7/2}$	$0f_{7/2}$	$0f_{7/2}$	$1p_{3/2}$	4	1	−0.408
$0f_{7/2}$	$1p_{3/2}$	$0f_{7/2}$	$1p_{3/2}$	4	1	0.059
$0f_{7/2}$	$1p_{3/2}$	$0f_{7/2}$	$1p_{3/2}$	5	1	0.497
$0f_{7/2}$	$0f_{7/2}$	$0f_{7/2}$	$0f_{7/2}$	6	1	0.406
$1p_{3/2}$	$1p_{3/2}$	$1p_{3/2}$	$1p_{3/2}$	0	−1	−0.748
$1p_{3/2}$	$1p_{3/2}$	$1p_{1/2}$	$1p_{1/2}$	0	−1	−0.903
$1p_{3/2}$	$1p_{3/2}$	$0f_{5/2}$	$0f_{5/2}$	0	−1	−0.712
$1p_{3/2}$	$1p_{3/2}$	$0g_{9/2}$	$0g_{9/2}$	0	−1	1.171
$1p_{1/2}$	$1p_{1/2}$	$1p_{1/2}$	$1p_{1/2}$	0	−1	−0.312
$1p_{1/2}$	$1p_{1/2}$	$0f_{5/2}$	$0f_{5/2}$	0	−1	−0.478
$1p_{1/2}$	$1p_{1/2}$	$0g_{9/2}$	$0g_{9/2}$	0	−1	0.884
$0f_{5/2}$	$0f_{5/2}$	$0f_{5/2}$	$0f_{5/2}$	0	−1	−0.988
$0f_{5/2}$	$0f_{5/2}$	$0g_{9/2}$	$0g_{9/2}$	0	−1	1.577
$0g_{9/2}$	$0g_{9/2}$	$0g_{9/2}$	$0g_{9/2}$	0	−1	−1.179
$1p_{3/2}$	$1p_{1/2}$	$1p_{3/2}$	$1p_{1/2}$	1	−1	0.167
$1p_{3/2}$	$1p_{1/2}$	$1p_{3/2}$	$0f_{5/2}$	1	−1	−0.054
$1p_{3/2}$	$0f_{5/2}$	$1p_{3/2}$	$0f_{5/2}$	1	−1	0.046
$1p_{3/2}$	$1p_{3/2}$	$1p_{3/2}$	$1p_{3/2}$	2	−1	−0.241
$1p_{3/2}$	$1p_{3/2}$	$1p_{3/2}$	$1p_{1/2}$	2	−1	−0.394
$1p_{3/2}$	$1p_{3/2}$	$1p_{3/2}$	$0f_{5/2}$	2	−1	−0.162
$1p_{3/2}$	$1p_{3/2}$	$1p_{1/2}$	$0f_{5/2}$	2	−1	−0.179
$1p_{3/2}$	$1p_{3/2}$	$0f_{5/2}$	$0f_{5/2}$	2	−1	−0.178
$1p_{3/2}$	$1p_{3/2}$	$0g_{9/2}$	$0g_{9/2}$	2	−1	0.441
$1p_{3/2}$	$1p_{1/2}$	$1p_{3/2}$	$1p_{1/2}$	2	−1	−0.448
$1p_{3/2}$	$1p_{1/2}$	$1p_{3/2}$	$0f_{5/2}$	2	−1	−0.176
$1p_{3/2}$	$1p_{1/2}$	$1p_{1/2}$	$0f_{5/2}$	2	−1	−0.407
$1p_{3/2}$	$1p_{1/2}$	$0f_{5/2}$	$0f_{5/2}$	2	−1	−0.292
$1p_{3/2}$	$1p_{1/2}$	$0g_{9/2}$	$0g_{9/2}$	2	−1	0.308
$1p_{3/2}$	$0f_{5/2}$	$1p_{3/2}$	$0f_{5/2}$	2	−1	0.071
$1p_{3/2}$	$0f_{5/2}$	$1p_{1/2}$	$0f_{5/2}$	2	−1	−0.280
$1p_{3/2}$	$0f_{5/2}$	$0f_{5/2}$	$0f_{5/2}$	2	−1	−0.103
$1p_{3/2}$	$0f_{5/2}$	$0g_{9/2}$	$0g_{9/2}$	2	−1	0.494
$1p_{1/2}$	$0f_{5/2}$	$1p_{1/2}$	$0f_{5/2}$	2	−1	−0.297
$1p_{1/2}$	$0f_{5/2}$	$0f_{5/2}$	$0f_{5/2}$	2	−1	−0.282
$1p_{1/2}$	$0f_{5/2}$	$0g_{9/2}$	$0g_{9/2}$	2	−1	0.572
$0f_{5/2}$	$0f_{5/2}$	$0f_{5/2}$	$0f_{5/2}$	2	−1	−0.405
$0f_{5/2}$	$0f_{5/2}$	$0g_{9/2}$	$0g_{9/2}$	2	−1	0.239
$0g_{9/2}$	$0g_{9/2}$	$0g_{9/2}$	$0g_{9/2}$	2	−1	−0.772
$1p_{3/2}$	$0f_{5/2}$	$1p_{3/2}$	$0f_{5/2}$	3	−1	0.125
$1p_{3/2}$	$0f_{5/2}$	$1p_{1/2}$	$0f_{5/2}$	3	−1	−0.005
$1p_{1/2}$	$0f_{5/2}$	$1p_{1/2}$	$0f_{5/2}$	3	−1	0.169
$1p_{3/2}$	$0f_{5/2}$	$1p_{3/2}$	$0f_{5/2}$	4	−1	−0.336
$1p_{3/2}$	$0f_{5/2}$	$0f_{5/2}$	$0f_{5/2}$	4	−1	−0.247
$1p_{3/2}$	$0f_{5/2}$	$0g_{9/2}$	$0g_{9/2}$	4	−1	0.493
$0f_{5/2}$	$0f_{5/2}$	$0f_{5/2}$	$0f_{5/2}$	4	−1	−0.087
$0f_{5/2}$	$0f_{5/2}$	$0g_{9/2}$	$0g_{9/2}$	4	−1	0.115
$0g_{9/2}$	$0g_{9/2}$	$0g_{9/2}$	$0g_{9/2}$	4	−1	−0.282
$0g_{9/2}$	$0g_{9/2}$	$0g_{9/2}$	$0g_{9/2}$	6	−1	−0.108
$0g_{9/2}$	$0g_{9/2}$	$0g_{9/2}$	$0g_{9/2}$	8	−1	−0.001
$0f_{5/2}$	$0g_{9/2}$	$0f_{5/2}$	$0g_{9/2}$	2	−1	−0.404
$1p_{3/2}$	$0g_{9/2}$	$1p_{3/2}$	$0g_{9/2}$	3	−1	−0.603
$1p_{3/2}$	$0g_{9/2}$	$0f_{5/2}$	$0g_{9/2}$	3	−1	0.227
$0f_{5/2}$	$0g_{9/2}$	$0f_{5/2}$	$0g_{9/2}$	3	−1	−0.211
$1p_{3/2}$	$0g_{9/2}$	$1p_{3/2}$	$0g_{9/2}$	4	−1	0.039
$1p_{3/2}$	$0g_{9/2}$	$1p_{1/2}$	$0g_{9/2}$	4	−1	−0.105
$1p_{3/2}$	$0g_{9/2}$	$0f_{5/2}$	$0g_{9/2}$	4	−1	0.157
$1p_{1/2}$	$0g_{9/2}$	$1p_{1/2}$	$0g_{9/2}$	4	−1	0.116
$1p_{1/2}$	$0g_{9/2}$	$0f_{5/2}$	$0g_{9/2}$	4	−1	−0.007
$0f_{5/2}$	$0g_{9/2}$	$0f_{5/2}$	$0g_{9/2}$	4	−1	0.109
$1p_{3/2}$	$0g_{9/2}$	$1p_{3/2}$	$0g_{9/2}$	5	−1	−0.099
$1p_{3/2}$	$0g_{9/2}$	$1p_{1/2}$	$0g_{9/2}$	5	−1	0.361
$1p_{3/2}$	$0g_{9/2}$	$0f_{5/2}$	$0g_{9/2}$	5	−1	0.158
$1p_{1/2}$	$0g_{9/2}$	$1p_{1/2}$	$0g_{9/2}$	5	−1	−0.335
$1p_{1/2}$	$0g_{9/2}$	$0f_{5/2}$	$0g_{9/2}$	5	−1	−0.252
$0f_{5/2}$	$0g_{9/2}$	$0f_{5/2}$	$0g_{9/2}$	5	−1	−0.065
$1p_{3/2}$	$0g_{9/2}$	$1p_{3/2}$	$0g_{9/2}$	6	−1	0.260
$1p_{3/2}$	$0g_{9/2}$	$0f_{5/2}$	$0g_{9/2}$	6	−1	0.176
$0f_{5/2}$	$0g_{9/2}$	$0f_{5/2}$	$0g_{9/2}$	6	−1	0.156
$0f_{5/2}$	$0g_{9/2}$	$0f_{5/2}$	$0g_{9/2}$	7	−1	−0.730
$1p_{3/2}$	$1p_{3/2}$	$1p_{3/2}$	$1p_{3/2}$	0	0	−2.071
$0f_{7/2}$	$0f_{5/2}$	$0f_{7/2}$	$0f_{5/2}$	1	0	−1.994
$0f_{7/2}$	$0f_{5/2}$	$1p_{3/2}$	$1p_{3/2}$	1	0	0.798
$0f_{7/2}$	$0f_{5/2}$	$1p_{3/2}$	$1p_{1/2}$	1	0	−0.970
$0f_{7/2}$	$0f_{5/2}$	$1p_{3/2}$	$0f_{5/2}$	1	0	−0.684
$1p_{3/2}$	$1p_{3/2}$	$1p_{3/2}$	$1p_{3/2}$	1	0	−0.388
$1p_{3/2}$	$1p_{3/2}$	$1p_{3/2}$	$1p_{1/2}$	1	0	0.617
$1p_{3/2}$	$1p_{3/2}$	$1p_{3/2}$	$0f_{5/2}$	1	0	−0.018
$1p_{3/2}$	$1p_{1/2}$	$1p_{3/2}$	$1p_{1/2}$	1	0	−0.742
$1p_{3/2}$	$1p_{1/2}$	$1p_{3/2}$	$0f_{5/2}$	1	0	−0.428
$1p_{3/2}$	$0f_{5/2}$	$1p_{3/2}$	$0f_{5/2}$	1	0	−1.046
$0f_{7/2}$	$1p_{3/2}$	$0f_{7/2}$	$1p_{3/2}$	2	0	−0.951
$0f_{7/2}$	$1p_{3/2}$	$0f_{7/2}$	$0f_{5/2}$	2	0	−0.738
$0f_{7/2}$	$1p_{3/2}$	$1p_{3/2}$	$1p_{3/2}$	2	0	−0.432
$0f_{7/2}$	$1p_{3/2}$	$1p_{3/2}$	$1p_{1/2}$	2	0	−0.758
$0f_{7/2}$	$1p_{3/2}$	$1p_{3/2}$	$0f_{5/2}$	2	0	−0.877
$0f_{7/2}$	$0f_{5/2}$	$0f_{7/2}$	$0f_{5/2}$	2	0	−1.424
$0f_{7/2}$	$0f_{5/2}$	$1p_{3/2}$	$1p_{3/2}$	2	0	−0.109
$0f_{7/2}$	$0f_{5/2}$	$1p_{3/2}$	$1p_{1/2}$	2	0	−0.641
$0f_{7/2}$	$0f_{5/2}$	$1p_{3/2}$	$0f_{5/2}$	2	0	−0.627
$1p_{3/2}$	$1p_{3/2}$	$1p_{3/2}$	$1p_{3/2}$	2	0	−0.547
$1p_{3/2}$	$1p_{3/2}$	$1p_{3/2}$	$1p_{1/2}$	2	0	−0.688
$1p_{3/2}$	$1p_{3/2}$	$1p_{3/2}$	$0f_{5/2}$	2	0	−0.165
$1p_{3/2}$	$1p_{1/2}$	$1p_{3/2}$	$1p_{1/2}$	2	0	−1.082
$1p_{3/2}$	$1p_{1/2}$	$1p_{3/2}$	$0f_{5/2}$	2	0	−0.443

TABLE III. (*Continued*.)

$n_a l_a j_a$	$n_b l_b j_b$	$n_c l_c j_c$	$n_d l_d j_d$	J	T_z	TBME
$1p_{3/2}$	$0f_{5/2}$	$1p_{3/2}$	$0f_{5/2}$	2	0	−0.447
$0f_{7/2}$	$1p_{3/2}$	$0f_{7/2}$	$1p_{3/2}$	3	0	−0.348
$0f_{7/2}$	$1p_{3/2}$	$0f_{7/2}$	$1p_{1/2}$	3	0	0.587
$0f_{7/2}$	$1p_{3/2}$	$0f_{7/2}$	$0f_{5/2}$	3	0	0.141
$0f_{7/2}$	$1p_{3/2}$	$1p_{3/2}$	$1p_{3/2}$	3	0	−0.449
$0f_{7/2}$	$1p_{3/2}$	$1p_{3/2}$	$0f_{5/2}$	3	0	0.141
$0f_{7/2}$	$1p_{1/2}$	$0f_{7/2}$	$1p_{1/2}$	3	0	−0.618
$0f_{7/2}$	$1p_{1/2}$	$0f_{7/2}$	$0f_{5/2}$	3	0	−0.275
$0f_{7/2}$	$1p_{1/2}$	$1p_{3/2}$	$1p_{3/2}$	3	0	0.528
$0f_{7/2}$	$1p_{1/2}$	$1p_{3/2}$	$0f_{5/2}$	3	0	−0.117
$0f_{7/2}$	$0f_{5/2}$	$0f_{7/2}$	$0f_{5/2}$	3	0	−0.524
$0f_{7/2}$	$0f_{5/2}$	$1p_{3/2}$	$1p_{3/2}$	3	0	0.436
$0f_{7/2}$	$0f_{5/2}$	$1p_{3/2}$	$0f_{5/2}$	3	0	−0.369
$1p_{3/2}$	$1p_{3/2}$	$1p_{3/2}$	$1p_{3/2}$	3	0	−0.811
$1p_{3/2}$	$1p_{3/2}$	$1p_{3/2}$	$0f_{5/2}$	3	0	0.227
$1p_{3/2}$	$0f_{5/2}$	$1p_{3/2}$	$0f_{5/2}$	3	0	−0.261
$0f_{7/2}$	$1p_{3/2}$	$0f_{7/2}$	$1p_{3/2}$	4	0	−0.100
$0f_{7/2}$	$1p_{3/2}$	$0f_{7/2}$	$1p_{1/2}$	4	0	−0.297
$0f_{7/2}$	$1p_{3/2}$	$0f_{7/2}$	$0f_{5/2}$	4	0	−0.229
$0f_{7/2}$	$1p_{3/2}$	$1p_{3/2}$	$0f_{5/2}$	4	0	−0.615
$0f_{7/2}$	$1p_{1/2}$	$0f_{7/2}$	$1p_{1/2}$	4	0	−0.592
$0f_{7/2}$	$1p_{1/2}$	$0f_{7/2}$	$0f_{5/2}$	4	0	−0.590
$0f_{7/2}$	$1p_{1/2}$	$1p_{3/2}$	$0f_{5/2}$	4	0	−1.004
$0f_{7/2}$	$0f_{5/2}$	$0f_{7/2}$	$0f_{5/2}$	4	0	−0.848
$0f_{7/2}$	$0f_{5/2}$	$1p_{3/2}$	$0f_{5/2}$	4	0	−0.783
$1p_{3/2}$	$0f_{5/2}$	$1p_{3/2}$	$0f_{5/2}$	4	0	−0.753
$0f_{7/2}$	$1p_{3/2}$	$0f_{7/2}$	$1p_{3/2}$	5	0	−0.884
$0f_{7/2}$	$1p_{3/2}$	$0f_{7/2}$	$0f_{5/2}$	5	0	0.274
$0f_{7/2}$	$0f_{5/2}$	$0f_{7/2}$	$0f_{5/2}$	5	0	−0.179
$0f_{7/2}$	$0f_{5/2}$	$0f_{7/2}$	$0f_{5/2}$	6	0	−1.577
$0f_{7/2}$	$0g_{9/2}$	$0f_{7/2}$	$0g_{9/2}$	1	0	−0.846
$0f_{7/2}$	$0g_{9/2}$	$0f_{7/2}$	$0g_{9/2}$	2	0	−0.617
$0f_{7/2}$	$0g_{9/2}$	$0f_{7/2}$	$0g_{9/2}$	3	0	−0.176
$0f_{7/2}$	$0g_{9/2}$	$1p_{3/2}$	$0g_{9/2}$	3	0	−0.419
$1p_{3/2}$	$0g_{9/2}$	$1p_{3/2}$	$0g_{9/2}$	3	0	−0.723
$0f_{7/2}$	$0g_{9/2}$	$0f_{7/2}$	$0g_{9/2}$	4	0	−0.091
$0f_{7/2}$	$0g_{9/2}$	$1p_{3/2}$	$0g_{9/2}$	4	0	−0.419
$1p_{3/2}$	$0g_{9/2}$	$1p_{3/2}$	$0g_{9/2}$	4	0	−0.211
$0f_{7/2}$	$0g_{9/2}$	$0f_{7/2}$	$0g_{9/2}$	5	0	−0.003
$0f_{7/2}$	$0g_{9/2}$	$1p_{3/2}$	$0g_{9/2}$	5	0	−0.282
$1p_{3/2}$	$0g_{9/2}$	$1p_{3/2}$	$0g_{9/2}$	5	0	−0.043
$0f_{7/2}$	$0g_{9/2}$	$0f_{7/2}$	$0g_{9/2}$	6	0	−0.149
$0f_{7/2}$	$0g_{9/2}$	$1p_{3/2}$	$0g_{9/2}$	6	0	−0.574
$1p_{3/2}$	$0g_{9/2}$	$1p_{3/2}$	$0g_{9/2}$	6	0	−0.533
$0f_{7/2}$	$0g_{9/2}$	$0f_{7/2}$	$0g_{9/2}$	7	0	0.073
$0f_{7/2}$	$0g_{9/2}$	$0f_{7/2}$	$0g_{9/2}$	8	0	−1.134

TABLE IV. Proton-proton, neutron-neutron, and proton-neutron matrix elements (in MeV) derived for calculations in model space (II). They are antisymmetrized and normalized by a factor $1/\sqrt{(1+\delta_{j_a j_b})(1+\delta_{j_c j_d})}$.

$n_a l_a j_a$	$n_b l_b j_b$	$n_c l_c j_c$	$n_d l_d j_d$	J	T_z	TBME
$0f_{7/2}$	$0f_{7/2}$	$0f_{7/2}$	$0f_{7/2}$	0	1	−2.026
$0f_{7/2}$	$0f_{7/2}$	$1p_{3/2}$	$1p_{3/2}$	0	1	−1.225
$1p_{3/2}$	$1p_{3/2}$	$1p_{3/2}$	$1p_{3/2}$	0	1	−0.068
$0f_{7/2}$	$0f_{7/2}$	$0f_{7/2}$	$0f_{7/2}$	2	1	−0.416
$0f_{7/2}$	$0f_{7/2}$	$0f_{7/2}$	$1p_{3/2}$	2	1	−0.710
$0f_{7/2}$	$0f_{7/2}$	$1p_{3/2}$	$1p_{3/2}$	2	1	−0.358
$0f_{7/2}$	$1p_{3/2}$	$0f_{7/2}$	$1p_{3/2}$	2	1	−0.556
$0f_{7/2}$	$1p_{3/2}$	$1p_{3/2}$	$1p_{3/2}$	2	1	−0.361
$1p_{3/2}$	$1p_{3/2}$	$1p_{3/2}$	$1p_{3/2}$	2	1	0.104
$0f_{7/2}$	$1p_{3/2}$	$0f_{7/2}$	$1p_{3/2}$	3	1	0.329
$0f_{7/2}$	$0f_{7/2}$	$0f_{7/2}$	$0f_{7/2}$	4	1	0.133
$0f_{7/2}$	$0f_{7/2}$	$0f_{7/2}$	$1p_{3/2}$	4	1	−0.410
$0f_{7/2}$	$1p_{3/2}$	$0f_{7/2}$	$1p_{3/2}$	4	1	0.057
$0f_{7/2}$	$1p_{3/2}$	$0f_{7/2}$	$1p_{3/2}$	5	1	0.496
$0f_{7/2}$	$0f_{7/2}$	$0f_{7/2}$	$0f_{7/2}$	6	1	0.407
$1p_{3/2}$	$1p_{3/2}$	$1p_{3/2}$	$1p_{3/2}$	0	−1	−0.715
$1p_{3/2}$	$1p_{3/2}$	$1p_{1/2}$	$1p_{1/2}$	0	−1	−0.869
$1p_{3/2}$	$1p_{3/2}$	$0f_{5/2}$	$0f_{5/2}$	0	−1	−0.695
$1p_{3/2}$	$1p_{3/2}$	$0g_{9/2}$	$0g_{9/2}$	0	−1	1.026
$1p_{3/2}$	$1p_{3/2}$	$1d_{5/2}$	$1d_{5/2}$	0	−1	0.967
$1p_{1/2}$	$1p_{1/2}$	$1p_{1/2}$	$1p_{1/2}$	0	−1	−0.302
$1p_{1/2}$	$1p_{1/2}$	$0f_{5/2}$	$0f_{5/2}$	0	−1	−0.470
$1p_{1/2}$	$1p_{1/2}$	$0g_{9/2}$	$0g_{9/2}$	0	−1	0.846
$1p_{1/2}$	$1p_{1/2}$	$1d_{5/2}$	$1d_{5/2}$	0	−1	0.603
$0f_{5/2}$	$0f_{5/2}$	$0f_{5/2}$	$0f_{5/2}$	0	−1	−0.978
$0f_{5/2}$	$0f_{5/2}$	$0g_{9/2}$	$0g_{9/2}$	0	−1	1.555
$0f_{5/2}$	$0f_{5/2}$	$1d_{5/2}$	$1d_{5/2}$	0	−1	0.610
$0g_{9/2}$	$0g_{9/2}$	$0g_{9/2}$	$0g_{9/2}$	0	−1	−1.171
$0g_{9/2}$	$0g_{9/2}$	$1d_{5/2}$	$1d_{5/2}$	0	−1	−0.884
$1d_{5/2}$	$1d_{5/2}$	$1d_{5/2}$	$1d_{5/2}$	0	−1	−0.904
$1p_{3/2}$	$1p_{1/2}$	$1p_{3/2}$	$1p_{1/2}$	1	−1	0.165
$1p_{3/2}$	$1p_{1/2}$	$1p_{3/2}$	$0f_{5/2}$	1	−1	−0.053
$1p_{3/2}$	$0f_{5/2}$	$1p_{3/2}$	$0f_{5/2}$	1	−1	0.050
$1p_{3/2}$	$1p_{3/2}$	$1p_{3/2}$	$1p_{3/2}$	2	−1	−0.219
$1p_{3/2}$	$1p_{3/2}$	$1p_{3/2}$	$1p_{1/2}$	2	−1	−0.372
$1p_{3/2}$	$1p_{3/2}$	$1p_{3/2}$	$0f_{5/2}$	2	−1	−0.158
$1p_{3/2}$	$1p_{3/2}$	$1p_{1/2}$	$0f_{5/2}$	2	−1	−0.163
$1p_{3/2}$	$1p_{3/2}$	$0f_{5/2}$	$0f_{5/2}$	2	−1	−0.168
$1p_{3/2}$	$1p_{3/2}$	$0g_{9/2}$	$0g_{9/2}$	2	−1	0.393
$1p_{3/2}$	$1p_{3/2}$	$0g_{9/2}$	$1d_{5/2}$	2	−1	0.340
$1p_{3/2}$	$1p_{3/2}$	$1d_{5/2}$	$1d_{5/2}$	2	−1	0.471
$1p_{3/2}$	$1p_{1/2}$	$1p_{3/2}$	$1p_{1/2}$	2	−1	−0.418
$1p_{3/2}$	$1p_{1/2}$	$1p_{3/2}$	$0f_{5/2}$	2	−1	−0.172
$1p_{3/2}$	$1p_{1/2}$	$1p_{1/2}$	$0f_{5/2}$	2	−1	−0.384
$1p_{3/2}$	$1p_{1/2}$	$0f_{5/2}$	$0f_{5/2}$	2	−1	−0.280
$1p_{3/2}$	$1p_{1/2}$	$0g_{9/2}$	$0g_{9/2}$	2	−1	0.271
$1p_{3/2}$	$1p_{1/2}$	$0g_{9/2}$	$1d_{5/2}$	2	−1	0.536
$1p_{3/2}$	$1p_{1/2}$	$1d_{5/2}$	$1d_{5/2}$	2	−1	0.207
$1p_{3/2}$	$0f_{5/2}$	$1p_{3/2}$	$0f_{5/2}$	2	−1	0.072
$1p_{3/2}$	$0f_{5/2}$	$1p_{1/2}$	$0f_{5/2}$	2	−1	−0.277
$1p_{3/2}$	$0f_{5/2}$	$0f_{5/2}$	$0f_{5/2}$	2	−1	−0.101
$1p_{3/2}$	$0f_{5/2}$	$0g_{9/2}$	$0g_{9/2}$	2	−1	0.475
$1p_{3/2}$	$0f_{5/2}$	$0g_{9/2}$	$1d_{5/2}$	2	−1	0.072
$1p_{3/2}$	$0f_{5/2}$	$1d_{5/2}$	$1d_{5/2}$	2	−1	0.089

TABLE IV. (*Continued*.)

$n_a l_a j_a$	$n_b l_b j_b$	$n_c l_c j_c$	$n_d l_d j_d$	J	T_z	TBME
$1p_{1/2}$	$0f_{5/2}$	$1p_{1/2}$	$0f_{5/2}$	2	−1	−0.277
$1p_{1/2}$	$0f_{5/2}$	$0f_{5/2}$	$0f_{5/2}$	2	−1	−0.273
$1p_{1/2}$	$0f_{5/2}$	$0g_{9/2}$	$0g_{9/2}$	2	−1	0.552
$1p_{1/2}$	$0f_{5/2}$	$0g_{9/2}$	$1d_{5/2}$	2	−1	0.526
$1p_{1/2}$	$0f_{5/2}$	$1d_{5/2}$	$1d_{5/2}$	2	−1	0.186
$0f_{5/2}$	$0f_{5/2}$	$0f_{5/2}$	$0f_{5/2}$	2	−1	−0.400
$0f_{5/2}$	$0f_{5/2}$	$0g_{9/2}$	$0g_{9/2}$	2	−1	0.229
$0f_{5/2}$	$0f_{5/2}$	$0g_{9/2}$	$1d_{5/2}$	2	−1	0.269
$0f_{5/2}$	$0f_{5/2}$	$1d_{5/2}$	$1d_{5/2}$	2	−1	0.138
$0g_{9/2}$	$0g_{9/2}$	$0g_{9/2}$	$0g_{9/2}$	2	−1	−0.756
$0g_{9/2}$	$0g_{9/2}$	$0g_{9/2}$	$1d_{5/2}$	2	−1	−0.377
$0g_{9/2}$	$0g_{9/2}$	$1d_{5/2}$	$1d_{5/2}$	2	−1	−0.347
$0g_{9/2}$	$1d_{5/2}$	$0g_{9/2}$	$1d_{5/2}$	2	−1	−0.774
$0g_{9/2}$	$1d_{5/2}$	$1d_{5/2}$	$1d_{5/2}$	2	−1	−0.361
$1d_{5/2}$	$1d_{5/2}$	$1d_{5/2}$	$1d_{5/2}$	2	−1	−0.275
$1p_{3/2}$	$0f_{5/2}$	$1p_{3/2}$	$0f_{5/2}$	3	−1	0.126
$1p_{3/2}$	$0f_{5/2}$	$1p_{1/2}$	$0f_{5/2}$	3	−1	−0.005
$1p_{3/2}$	$0f_{5/2}$	$0g_{9/2}$	$1d_{5/2}$	3	−1	0.069
$1p_{1/2}$	$0f_{5/2}$	$1p_{1/2}$	$0f_{5/2}$	3	−1	0.172
$1p_{1/2}$	$0f_{5/2}$	$0g_{9/2}$	$1d_{5/2}$	3	−1	0.125
$0g_{9/2}$	$1d_{5/2}$	$0g_{9/2}$	$1d_{5/2}$	3	−1	−0.138
$1p_{3/2}$	$0f_{5/2}$	$1p_{3/2}$	$0f_{5/2}$	4	−1	−0.326
$1p_{3/2}$	$0f_{5/2}$	$0f_{5/2}$	$0f_{5/2}$	4	−1	−0.244
$1p_{3/2}$	$0f_{5/2}$	$0g_{9/2}$	$0g_{9/2}$	4	−1	0.469
$1p_{3/2}$	$0f_{5/2}$	$0g_{9/2}$	$1d_{5/2}$	4	−1	0.350
$1p_{3/2}$	$0f_{5/2}$	$1d_{5/2}$	$1d_{5/2}$	4	−1	0.089
$0f_{5/2}$	$0f_{5/2}$	$0f_{5/2}$	$0f_{5/2}$	4	−1	−0.086
$0f_{5/2}$	$0f_{5/2}$	$0g_{9/2}$	$0g_{9/2}$	4	−1	0.109
$0f_{5/2}$	$0f_{5/2}$	$0g_{9/2}$	$1d_{5/2}$	4	−1	0.097
$0f_{5/2}$	$0f_{5/2}$	$1d_{5/2}$	$1d_{5/2}$	4	−1	0.089
$0g_{9/2}$	$0g_{9/2}$	$0g_{9/2}$	$0g_{9/2}$	4	−1	−0.273
$0g_{9/2}$	$0g_{9/2}$	$0g_{9/2}$	$1d_{5/2}$	4	−1	−0.357
$0g_{9/2}$	$0g_{9/2}$	$1d_{5/2}$	$1d_{5/2}$	4	−1	−0.156
$0g_{9/2}$	$1d_{5/2}$	$0g_{9/2}$	$1d_{5/2}$	4	−1	−0.229
$0g_{9/2}$	$1d_{5/2}$	$1d_{5/2}$	$1d_{5/2}$	4	−1	−0.204
$1d_{5/2}$	$1d_{5/2}$	$1d_{5/2}$	$1d_{5/2}$	4	−1	−0.072
$0g_{9/2}$	$1d_{5/2}$	$0g_{9/2}$	$1d_{5/2}$	5	−1	0.121
$0g_{9/2}$	$0g_{9/2}$	$0g_{9/2}$	$0g_{9/2}$	6	−1	−0.105
$0g_{9/2}$	$0g_{9/2}$	$0g_{9/2}$	$1d_{5/2}$	6	−1	−0.234
$0g_{9/2}$	$1d_{5/2}$	$0g_{9/2}$	$1d_{5/2}$	6	−1	−0.031
$0g_{9/2}$	$1d_{5/2}$	$0g_{9/2}$	$1d_{5/2}$	7	−1	0.127
$0g_{9/2}$	$0g_{9/2}$	$0g_{9/2}$	$0g_{9/2}$	8	−1	−0.001
$0f_{5/2}$	$1d_{5/2}$	$0f_{5/2}$	$1d_{5/2}$	0	−1	−0.497
$1p_{3/2}$	$1d_{5/2}$	$1p_{3/2}$	$1d_{5/2}$	1	−1	−0.765
$1p_{3/2}$	$1d_{5/2}$	$0f_{5/2}$	$1d_{5/2}$	1	−1	0.246
$0f_{5/2}$	$1d_{5/2}$	$0f_{5/2}$	$1d_{5/2}$	1	−1	−0.089
$1p_{3/2}$	$1d_{5/2}$	$1p_{3/2}$	$1d_{5/2}$	2	−1	−0.080
$1p_{3/2}$	$1d_{5/2}$	$1p_{1/2}$	$1d_{5/2}$	2	−1	−0.103
$1p_{3/2}$	$1d_{5/2}$	$0f_{5/2}$	$0g_{9/2}$	2	−1	−0.293
$1p_{3/2}$	$1d_{5/2}$	$0f_{5/2}$	$1d_{5/2}$	2	−1	0.032
$1p_{1/2}$	$1d_{5/2}$	$1p_{1/2}$	$1d_{5/2}$	2	−1	−0.072
$1p_{1/2}$	$1d_{5/2}$	$0f_{5/2}$	$0g_{9/2}$	2	−1	−0.348
$1p_{1/2}$	$1d_{5/2}$	$0f_{5/2}$	$1d_{5/2}$	2	−1	−0.123
$0f_{5/2}$	$0g_{9/2}$	$0f_{5/2}$	$0g_{9/2}$	2	−1	−0.382
$0f_{5/2}$	$0g_{9/2}$	$0f_{5/2}$	$1d_{5/2}$	2	−1	−0.216
$0f_{5/2}$	$1d_{5/2}$	$0f_{5/2}$	$1d_{5/2}$	2	−1	−0.057
$1p_{3/2}$	$0g_{9/2}$	$1p_{3/2}$	$0g_{9/2}$	3	−1	−0.497

TABLE IV. (*Continued*.)

$n_a l_a j_a$	$n_b l_b j_b$	$n_c l_c j_c$	$n_d l_d j_d$	J	T_z	TBME
$1p_{3/2}$	$0g_{9/2}$	$1p_{3/2}$	$1d_{5/2}$	3	−1	−0.337
$1p_{3/2}$	$0g_{9/2}$	$1p_{1/2}$	$1d_{5/2}$	3	−1	0.420
$1p_{3/2}$	$0g_{9/2}$	$0f_{5/2}$	$0g_{9/2}$	3	−1	0.199
$1p_{3/2}$	$0g_{9/2}$	$0f_{5/2}$	$1d_{5/2}$	3	−1	0.285
$1p_{3/2}$	$1d_{5/2}$	$1p_{3/2}$	$1d_{5/2}$	3	−1	−0.386
$1p_{3/2}$	$1d_{5/2}$	$1p_{1/2}$	$1d_{5/2}$	3	−1	0.315
$1p_{3/2}$	$1d_{5/2}$	$0f_{5/2}$	$0g_{9/2}$	3	−1	0.023
$1p_{3/2}$	$1d_{5/2}$	$0f_{5/2}$	$1d_{5/2}$	3	−1	0.182
$1p_{1/2}$	$1d_{5/2}$	$1p_{1/2}$	$1d_{5/2}$	3	−1	−0.416
$1p_{1/2}$	$1d_{5/2}$	$0f_{5/2}$	$0g_{9/2}$	3	−1	−0.274
$1p_{1/2}$	$1d_{5/2}$	$0f_{5/2}$	$1d_{5/2}$	3	−1	−0.240
$0f_{5/2}$	$0g_{9/2}$	$0f_{5/2}$	$0g_{9/2}$	3	−1	−0.194
$0f_{5/2}$	$0g_{9/2}$	$0f_{5/2}$	$1d_{5/2}$	3	−1	−0.300
$0f_{5/2}$	$1d_{5/2}$	$0f_{5/2}$	$1d_{5/2}$	3	−1	−0.014
$1p_{3/2}$	$0g_{9/2}$	$1p_{3/2}$	$0g_{9/2}$	4	−1	0.054
$1p_{3/2}$	$0g_{9/2}$	$1p_{3/2}$	$1d_{5/2}$	4	−1	−0.024
$1p_{3/2}$	$0g_{9/2}$	$1p_{1/2}$	$0g_{9/2}$	4	−1	−0.105
$1p_{3/2}$	$0g_{9/2}$	$0f_{5/2}$	$0g_{9/2}$	4	−1	0.151
$1p_{3/2}$	$0g_{9/2}$	$0f_{5/2}$	$1d_{5/2}$	4	−1	0.076
$1p_{3/2}$	$1d_{5/2}$	$1p_{3/2}$	$1d_{5/2}$	4	−1	0.257
$1p_{3/2}$	$1d_{5/2}$	$1p_{1/2}$	$0g_{9/2}$	4	−1	−0.035
$1p_{3/2}$	$1d_{5/2}$	$0f_{5/2}$	$0g_{9/2}$	4	−1	−0.128
$1p_{3/2}$	$1d_{5/2}$	$0f_{5/2}$	$1d_{5/2}$	4	−1	−0.018
$1p_{1/2}$	$0g_{9/2}$	$1p_{1/2}$	$0g_{9/2}$	4	−1	0.113
$1p_{1/2}$	$0g_{9/2}$	$0f_{5/2}$	$0g_{9/2}$	4	−1	−0.009
$1p_{1/2}$	$0g_{9/2}$	$0f_{5/2}$	$1d_{5/2}$	4	−1	0.022
$0f_{5/2}$	$0g_{9/2}$	$0f_{5/2}$	$0g_{9/2}$	4	−1	0.116
$0f_{5/2}$	$0g_{9/2}$	$0f_{5/2}$	$1d_{5/2}$	4	−1	−0.137
$0f_{5/2}$	$1d_{5/2}$	$0f_{5/2}$	$1d_{5/2}$	4	−1	0.027
$1p_{3/2}$	$0g_{9/2}$	$1p_{3/2}$	$0g_{9/2}$	5	−1	−0.075
$1p_{3/2}$	$0g_{9/2}$	$1p_{1/2}$	$0g_{9/2}$	5	−1	0.333
$1p_{3/2}$	$0g_{9/2}$	$0f_{5/2}$	$0g_{9/2}$	5	−1	0.136
$1p_{3/2}$	$0g_{9/2}$	$0f_{5/2}$	$1d_{5/2}$	5	−1	0.347
$1p_{1/2}$	$0g_{9/2}$	$1p_{1/2}$	$0g_{9/2}$	5	−1	−0.309
$1p_{1/2}$	$0g_{9/2}$	$0f_{5/2}$	$0g_{9/2}$	5	−1	−0.233
$1p_{1/2}$	$0g_{9/2}$	$0f_{5/2}$	$1d_{5/2}$	5	−1	−0.449
$0f_{5/2}$	$0g_{9/2}$	$0f_{5/2}$	$0g_{9/2}$	5	−1	−0.050
$0f_{5/2}$	$0g_{9/2}$	$0f_{5/2}$	$1d_{5/2}$	5	−1	−0.418
$0f_{5/2}$	$1d_{5/2}$	$0f_{5/2}$	$1d_{5/2}$	5	−1	−0.373
$1p_{3/2}$	$0g_{9/2}$	$1p_{3/2}$	$0g_{9/2}$	6	−1	0.267
$1p_{3/2}$	$0g_{9/2}$	$0f_{5/2}$	$0g_{9/2}$	6	−1	0.176
$0f_{5/2}$	$0g_{9/2}$	$0f_{5/2}$	$0g_{9/2}$	6	−1	0.158
$0f_{5/2}$	$0g_{9/2}$	$0f_{5/2}$	$0g_{9/2}$	7	−1	−0.719
$1p_{3/2}$	$1p_{3/2}$	$1p_{3/2}$	$1p_{3/2}$	0	0	−2.101
$0f_{7/2}$	$0f_{5/2}$	$0f_{7/2}$	$0f_{5/2}$	1	0	−2.000
$0f_{7/2}$	$0f_{5/2}$	$1p_{3/2}$	$1p_{3/2}$	1	0	0.804
$0f_{7/2}$	$0f_{5/2}$	$1p_{3/2}$	$1p_{1/2}$	1	0	−0.977
$0f_{7/2}$	$0f_{5/2}$	$1p_{3/2}$	$0f_{5/2}$	1	0	−0.680
$1p_{3/2}$	$1p_{3/2}$	$1p_{3/2}$	$1p_{3/2}$	1	0	−0.387
$1p_{3/2}$	$1p_{3/2}$	$1p_{3/2}$	$1p_{1/2}$	1	0	0.618
$1p_{3/2}$	$1p_{3/2}$	$1p_{3/2}$	$0f_{5/2}$	1	0	−0.019
$1p_{3/2}$	$1p_{1/2}$	$1p_{3/2}$	$1p_{1/2}$	1	0	−0.742
$1p_{3/2}$	$1p_{1/2}$	$1p_{3/2}$	$0f_{5/2}$	1	0	−0.422
$1p_{3/2}$	$0f_{5/2}$	$1p_{3/2}$	$0f_{5/2}$	1	0	−1.036
$0f_{7/2}$	$1p_{3/2}$	$0f_{7/2}$	$1p_{3/2}$	2	0	−1.004
$0f_{7/2}$	$1p_{3/2}$	$0f_{7/2}$	$0f_{5/2}$	2	0	−0.748
$0f_{7/2}$	$1p_{3/2}$	$1p_{3/2}$	$1p_{3/2}$	2	0	−0.455

TABLE IV. (*Continued*.)

$n_a l_a j_a$	$n_b l_b j_b$	$n_c l_c j_c$	$n_d l_d j_d$	J	T_z	TBME
$0f_{7/2}$	$1p_{3/2}$	$1p_{3/2}$	$1p_{1/2}$	2	0	−0.801
$0f_{7/2}$	$1p_{3/2}$	$1p_{3/2}$	$0f_{5/2}$	2	0	−0.900
$0f_{7/2}$	$0f_{5/2}$	$0f_{7/2}$	$0f_{5/2}$	2	0	−1.422
$0f_{7/2}$	$0f_{5/2}$	$1p_{3/2}$	$1p_{3/2}$	2	0	−0.111
$0f_{7/2}$	$0f_{5/2}$	$1p_{3/2}$	$1p_{1/2}$	2	0	−0.648
$0f_{7/2}$	$0f_{5/2}$	$1p_{3/2}$	$0f_{5/2}$	2	0	−0.631
$1p_{3/2}$	$1p_{3/2}$	$1p_{3/2}$	$1p_{3/2}$	2	0	−0.555
$1p_{3/2}$	$1p_{3/2}$	$1p_{3/2}$	$1p_{1/2}$	2	0	−0.699
$1p_{3/2}$	$1p_{3/2}$	$1p_{3/2}$	$0f_{5/2}$	2	0	−0.176
$1p_{3/2}$	$1p_{1/2}$	$1p_{3/2}$	$1p_{1/2}$	2	0	−1.104
$1p_{3/2}$	$1p_{1/2}$	$1p_{3/2}$	$0f_{5/2}$	2	0	−0.462
$1p_{3/2}$	$0f_{5/2}$	$1p_{3/2}$	$0f_{5/2}$	2	0	−0.457
$0f_{7/2}$	$1p_{3/2}$	$0f_{7/2}$	$1p_{3/2}$	3	0	−0.370
$0f_{7/2}$	$1p_{3/2}$	$0f_{7/2}$	$1p_{1/2}$	3	0	0.603
$0f_{7/2}$	$1p_{3/2}$	$0f_{7/2}$	$0f_{5/2}$	3	0	0.144
$0f_{7/2}$	$1p_{3/2}$	$1p_{3/2}$	$1p_{3/2}$	3	0	−0.473
$0f_{7/2}$	$1p_{3/2}$	$1p_{3/2}$	$0f_{5/2}$	3	0	0.142
$0f_{7/2}$	$1p_{1/2}$	$0f_{7/2}$	$1p_{1/2}$	3	0	−0.628
$0f_{7/2}$	$1p_{1/2}$	$0f_{7/2}$	$0f_{5/2}$	3	0	−0.279
$0f_{7/2}$	$1p_{1/2}$	$1p_{3/2}$	$1p_{3/2}$	3	0	0.544
$0f_{7/2}$	$1p_{1/2}$	$1p_{3/2}$	$0f_{5/2}$	3	0	−0.119
$0f_{7/2}$	$0f_{5/2}$	$0f_{7/2}$	$0f_{5/2}$	3	0	−0.525
$0f_{7/2}$	$0f_{5/2}$	$1p_{3/2}$	$1p_{3/2}$	3	0	0.439
$0f_{7/2}$	$0f_{5/2}$	$1p_{3/2}$	$0f_{5/2}$	3	0	−0.369
$1p_{3/2}$	$1p_{3/2}$	$1p_{3/2}$	$1p_{3/2}$	3	0	−0.826
$1p_{3/2}$	$1p_{3/2}$	$1p_{3/2}$	$0f_{5/2}$	3	0	0.227
$1p_{3/2}$	$0f_{5/2}$	$1p_{3/2}$	$0f_{5/2}$	3	0	−0.258
$0f_{7/2}$	$1p_{3/2}$	$0f_{7/2}$	$1p_{3/2}$	4	0	−0.106
$0f_{7/2}$	$1p_{3/2}$	$0f_{7/2}$	$1p_{1/2}$	4	0	−0.302
$0f_{7/2}$	$1p_{3/2}$	$0f_{7/2}$	$0f_{5/2}$	4	0	−0.229
$0f_{7/2}$	$1p_{3/2}$	$1p_{3/2}$	$0f_{5/2}$	4	0	−0.620
$0f_{7/2}$	$1p_{1/2}$	$0f_{7/2}$	$1p_{1/2}$	4	0	−0.593
$0f_{7/2}$	$1p_{1/2}$	$0f_{7/2}$	$0f_{5/2}$	4	0	−0.590
$0f_{7/2}$	$1p_{1/2}$	$1p_{3/2}$	$0f_{5/2}$	4	0	−1.006
$0f_{7/2}$	$0f_{5/2}$	$0f_{7/2}$	$0f_{5/2}$	4	0	−0.843
$0f_{7/2}$	$0f_{5/2}$	$1p_{3/2}$	$0f_{5/2}$	4	0	−0.782
$1p_{3/2}$	$0f_{5/2}$	$1p_{3/2}$	$0f_{5/2}$	4	0	−0.756
$0f_{7/2}$	$1p_{3/2}$	$0f_{7/2}$	$1p_{3/2}$	5	0	−0.916
$0f_{7/2}$	$1p_{3/2}$	$0f_{7/2}$	$0f_{5/2}$	5	0	0.282
$0f_{7/2}$	$0f_{5/2}$	$0f_{7/2}$	$0f_{5/2}$	5	0	−0.184
$0f_{7/2}$	$0f_{5/2}$	$0f_{7/2}$	$0f_{5/2}$	6	0	−1.570
$0f_{7/2}$	$0g_{9/2}$	$0f_{7/2}$	$0g_{9/2}$	1	0	−0.843
$0f_{7/2}$	$0g_{9/2}$	$0f_{7/2}$	$1d_{5/2}$	1	0	−0.191
$0f_{7/2}$	$0g_{9/2}$	$1p_{3/2}$	$1d_{5/2}$	1	0	−0.674
$0f_{7/2}$	$1d_{5/2}$	$0f_{7/2}$	$1d_{5/2}$	1	0	−0.636
$0f_{7/2}$	$1d_{5/2}$	$1p_{3/2}$	$1d_{5/2}$	1	0	−0.248
$1p_{3/2}$	$1d_{5/2}$	$1p_{3/2}$	$1d_{5/2}$	1	0	−0.847
$0f_{7/2}$	$0g_{9/2}$	$0f_{7/2}$	$0g_{9/2}$	2	0	−0.590
$0f_{7/2}$	$0g_{9/2}$	$0f_{7/2}$	$1d_{5/2}$	2	0	−0.454
$0f_{7/2}$	$0g_{9/2}$	$1p_{3/2}$	$1d_{5/2}$	2	0	−0.405
$0f_{7/2}$	$1d_{5/2}$	$0f_{7/2}$	$1d_{5/2}$	2	0	−0.443
$0f_{7/2}$	$1d_{5/2}$	$1p_{3/2}$	$1d_{5/2}$	2	0	−0.437
$1p_{3/2}$	$1d_{5/2}$	$1p_{3/2}$	$1d_{5/2}$	2	0	−0.488
$0f_{7/2}$	$0g_{9/2}$	$0f_{7/2}$	$0g_{9/2}$	3	0	−0.179
$0f_{7/2}$	$0g_{9/2}$	$0f_{7/2}$	$1d_{5/2}$	3	0	−0.229
$0f_{7/2}$	$0g_{9/2}$	$1p_{3/2}$	$0g_{9/2}$	3	0	−0.436
$0f_{7/2}$	$0g_{9/2}$	$1p_{3/2}$	$1d_{5/2}$	3	0	−0.218

TABLE IV. (*Continued*.)

$n_a l_a j_a$	$n_b l_b j_b$	$n_c l_c j_c$	$n_d l_d j_d$	J	T_z	TBME
$0f_{7/2}$	$1d_{5/2}$	$0f_{7/2}$	$1d_{5/2}$	3	0	−0.108
$0f_{7/2}$	$1d_{5/2}$	$1p_{3/2}$	$0g_{9/2}$	3	0	−0.211
$0f_{7/2}$	$1d_{5/2}$	$1p_{3/2}$	$1d_{5/2}$	3	0	−0.213
$1p_{3/2}$	$0g_{9/2}$	$1p_{3/2}$	$0g_{9/2}$	3	0	−0.772
$1p_{3/2}$	$0g_{9/2}$	$1p_{3/2}$	$1d_{5/2}$	3	0	−0.378
$1p_{3/2}$	$1d_{5/2}$	$1p_{3/2}$	$1d_{5/2}$	3	0	−0.250
$0f_{7/2}$	$0g_{9/2}$	$0f_{7/2}$	$0g_{9/2}$	4	0	−0.070
$0f_{7/2}$	$0g_{9/2}$	$0f_{7/2}$	$1d_{5/2}$	4	0	−0.351
$0f_{7/2}$	$0g_{9/2}$	$1p_{3/2}$	$0g_{9/2}$	4	0	−0.397
$0f_{7/2}$	$0g_{9/2}$	$1p_{3/2}$	$1d_{5/2}$	4	0	−0.357
$0f_{7/2}$	$1d_{5/2}$	$0f_{7/2}$	$1d_{5/2}$	4	0	−0.254
$0f_{7/2}$	$1d_{5/2}$	$1p_{3/2}$	$0g_{9/2}$	4	0	−0.329
$0f_{7/2}$	$1d_{5/2}$	$1p_{3/2}$	$1d_{5/2}$	4	0	−0.483
$1p_{3/2}$	$0g_{9/2}$	$1p_{3/2}$	$0g_{9/2}$	4	0	−0.190
$1p_{3/2}$	$0g_{9/2}$	$1p_{3/2}$	$1d_{5/2}$	4	0	−0.409
$1p_{3/2}$	$1d_{5/2}$	$1p_{3/2}$	$1d_{5/2}$	4	0	−0.770
$0f_{7/2}$	$0g_{9/2}$	$0f_{7/2}$	$0g_{9/2}$	5	0	−0.015
$0f_{7/2}$	$0g_{9/2}$	$0f_{7/2}$	$1d_{5/2}$	5	0	−0.147
$0f_{7/2}$	$0g_{9/2}$	$1p_{3/2}$	$0g_{9/2}$	5	0	−0.297
$0f_{7/2}$	$1d_{5/2}$	$0f_{7/2}$	$1d_{5/2}$	5	0	−0.029
$0f_{7/2}$	$1d_{5/2}$	$1p_{3/2}$	$0g_{9/2}$	5	0	−0.134
$1p_{3/2}$	$0g_{9/2}$	$1p_{3/2}$	$0g_{9/2}$	5	0	−0.069
$0f_{7/2}$	$0g_{9/2}$	$0f_{7/2}$	$0g_{9/2}$	6	0	−0.125
$0f_{7/2}$	$0g_{9/2}$	$0f_{7/2}$	$1d_{5/2}$	6	0	−0.447
$0f_{7/2}$	$0g_{9/2}$	$1p_{3/2}$	$0g_{9/2}$	6	0	−0.538
$0f_{7/2}$	$1d_{5/2}$	$0f_{7/2}$	$1d_{5/2}$	6	0	−0.742
$0f_{7/2}$	$1d_{5/2}$	$1p_{3/2}$	$0g_{9/2}$	6	0	−0.671
$1p_{3/2}$	$0g_{9/2}$	$1p_{3/2}$	$0g_{9/2}$	6	0	−0.479
$0f_{7/2}$	$0g_{9/2}$	$0f_{7/2}$	$0g_{9/2}$	7	0	0.063
$0f_{7/2}$	$0g_{9/2}$	$0f_{7/2}$	$0g_{9/2}$	8	0	−1.119

TABLE V. Proton effective charges of the electric quadrupole operator $E2$ for the model spaces (I) and (II).

$n_a l_a j_a$	$n_b l_b j_b$	$\langle a\|\|e_n\|\|b\rangle$ (I)	$\langle a\|\|e_n\|\|b\rangle$ (II)
$0f_{7/2}$	$0f_{7/2}$	1.22	1.23
$0f_{7/2}$	$1p_{3/2}$	1.34	1.36
$1p_{3/2}$	$1p_{3/2}$	1.40	1.42

TABLE VI. Neutron effective charges of the electric quadrupole operator $E2$ for the model spaces (I) and (II).

$n_a l_a j_a$	$n_b l_b j_b$	$\langle a\|\|e_n\|\|b\rangle$ (I)	$\langle a\|\|e_n\|\|b\rangle$ (II)
$1p_{3/2}$	$1p_{3/2}$	0.38	0.40
$1p_{3/2}$	$1p_{1/2}$	0.39	0.42
$1p_{3/2}$	$0f_{5/2}$	0.43	0.46
$1p_{1/2}$	$0f_{5/2}$	0.41	0.45
$0f_{5/2}$	$0f_{5/2}$	0.59	0.61
$0g_{9/2}$	$0g_{9/2}$	0.39	0.40
$0g_{9/2}$	$1d_{5/2}$		0.35
$1d_{5/2}$	$1d_{5/2}$		0.36

TABLE VII. Occupation numbers of proton $0f_{7/2}$ and neutron $0g_{9/2}, 1d_{5/2}$ of $^{56-62}$Ti, $^{58-64}$Cr, $^{60-66}$Fe, and $^{62-68}$Ni calculated with model spaces (I) and (II) (see text for details).

	$N=34$		$N=36$		$N=38$		$N=40$	
	(I)	(II)	(I)	(II)	(I)	(II)	(I)	(II)
				Ti				
$\pi 0f_{7/2}$	1.71	1.71	1.84	1.72	1.87	1.71	1.87	1.69
$\nu 0g_{9/2}$	0.24	0.31	0.95	1.45	2.15	2.61	3.23	3.72
$\nu 1d_{5/2}$		0.05		0.17		0.27		0.36
				Cr				
$\pi 0f_{7/2}$	3.37	3.37	3.54	3.33	3.60	3.26	3.64	3.31
$\nu 0g_{9/2}$	0.14	0.18	0.66	1.48	1.68	2.98	2.88	3.73
$\nu 1d_{5/2}$		0.04		0.26		0.53		0.57
				Fe				
$\pi 0f_{7/2}$	5.36	5.35	5.35	5.34	5.49	5.31	5.61	5.31
$\nu 0g_{9/2}$	0.10	0.12	0.27	0.37	0.89	1.51	1.75	2.81
$\nu 1d_{5/2}$		0.03		0.06		0.17		0.33
				Ni				
$\pi 0f_{7/2}$	6.77	6.76	6.92	6.91	7.33	7.32	7.89	7.85
$\nu 0g_{9/2}$	0.09	0.10	0.16	0.17	0.25	0.26	0.42	0.47
$\nu 1d_{5/2}$		0.02		0.03		0.04		0.05

[1] T. Otsuka, R. Fujimoto, Y. Utsuno, B. A. Brown, M. Honma, and T. Mizusaki, Phys. Rev. Lett. **87**, 082502 (2001).

[2] T. Otsuka, T. Suzuki, R. Fujimoto, H. Grawe, and Y. Akaishi, Phys. Rev. Lett. **95**, 232502 (2005).

[3] T. Otsuka, T. Suzuki, M. Honma, Y. Utsuno, N. Tsunoda, K. Tsukiyama, and M. Hjorth-Jensen, Phys. Rev. Lett. **104**, 012501 (2010).

[4] B. A. Brown, Physics **3**, 104 (2010).

[5] O. Sorlin, C. Donzaud, F. Nowacki, J. Angélique, F. Azaiez, C. Bourgeois, V. Chiste, Z. Dlouhy, S. Grévy, D. Guillemaud-Mueller *et al.*, Eur. Phys. J. A **16**, 55 (2003).

[6] P. Adrich, A. M. Amthor, D. Bazin, M. D. Bowen, B. A. Brown, C. M. Campbell, J. M. Cook, A. Gade, D. Galaviz, T. Glasmacher *et al.*, Phys. Rev. C **77**, 054306 (2008).

[7] J. Ljungvall, A. Görgen, A. Obertelli, W. Korten, E. Clément, G. de France, A. Bürger, J.-P. Delaroche, A. Dewald, A. Gadea *et al.*, Phys. Rev. C **81**, 061301 (2010).

[8] W. Rother, A. Dewald, H. Iwasaki, S. M. Lenzi, K. Starosta, D. Bazin, T. Baugher, B. A. Brown, H. L. Crawford, C. Fransen *et al.*, Phys. Rev. Lett. **106**, 022502 (2011).

[9] T. Baugher, A. Gade, R. V. F. Janssens, S. M. Lenzi, D. Bazin, B. A. Brown, M. P. Carpenter, A. N. Deacon, S. J. Freeman, T. Glasmacher *et al.*, Phys. Rev. C **86**, 011305 (2012).

[10] N. Aoi, E. Takeshita, H. Suzuki, S. Takeuchi, S. Ota, H. Baba, S. Bishop, T. Fukui, Y. Hashimoto, H. J. Ong *et al.*, Phys. Rev. Lett. **102**, 012502 (2009).

[11] A. Gade, R. V. F. Janssens, T. Baugher, D. Bazin, B. A. Brown, M. P. Carpenter, C. J. Chiara, A. N. Deacon, S. J. Freeman, G. F. Grinyer *et al.*, Phys. Rev. C **81**, 051304 (2010).

[12] A. P. Zuker, J. Retamosa, A. Poves, and E. Caurier, Phys. Rev. C **52**, R1741 (1995).

[13] E. Caurier, F. Nowacki, and A. Poves, Eur. Phys. J. A **15**, 145 (2002).

[14] S. M. Lenzi, F. Nowacki, A. Poves, and K. Sieja, Phys. Rev. C **82**, 054301 (2010).

[15] N. A. Smirnova, K. Heyde, B. Bally, F. Nowacki, and K. Sieja, Phys. Rev. C **86**, 034314 (2012).

[16] A. Schwenk and A. P. Zuker, Phys. Rev. C **74**, 061302 (2006).

[17] J. D. Holt, J. Menéndez, and A. Schwenk, J. Phys. G **40**, 075105 (2013).

[18] L. Coraggio, A. Covello, A. Gargano, N. Itaco, and T. T. S. Kuo, Prog. Part. Nucl. Phys. **62**, 135 (2009).

[19] S. Bogner, T. T. S. Kuo, and L. Coraggio, Nucl. Phys. A **684**, 432c (2001).

[20] S. Bogner, T. T. S. Kuo, L. Coraggio, A. Covello, and N. Itaco, Phys. Rev. C **65**, 051301(R) (2002).

[21] T. T. S. Kuo and E. Osnes, *Lecture Notes in Physics* (Springer-Verlag, Berlin, 1990), Vol. 364.

[22] T. T. S. Kuo, S. Y. Lee, and K. F. Ratcliff, Nucl. Phys. A **176**, 65 (1971).

[23] T. T. S. Kuo, J. Shurpin, K. C. Tam, E. Osnes, and P. J. Ellis, Ann. Phys. (NY) **132**, 237 (1981).

[24] L. Coraggio, A. Covello, A. Gargano, N. Itaco, and T. T. S. Kuo, Ann. Phys. (NY) **327**, 2125 (2012).

[25] G. A. Baker and J. L. Gammel, *The Padé Approximant in Theoretical Physics*, Vol. 71 of *Mathematics in Science and Engineering* (Academic Press, New York, 1970).

[26] N. Ayoub and H. A. Mavromatis, Nucl. Phys. A **323**, 125 (1979).

[27] H. M. Hoffmann, Y. Starkand, and M. W. Kirson, Nucl. Phys. A **266**, 138 (1976).

[28] K. Suzuki and S. Y. Lee, Prog. Theor. Phys. **64**, 2091 (1980).

[29] J. Shurpin, T. T. S. Kuo, and D. Strottman, Nucl. Phys. A **408**, 310 (1983).

[30] Data extracted using the NNDC On-line Data Service from the ENSDF database, file revised as of September 12, 2013.

[31] S. Fortier, I. Fodor-Lovas, E. Hourani, J. M. Maison, and J. P. Schapira, Nucl. Phys. A **346**, 303 (1980).
[32] P. D. Cottle and K. W. Kemper, Phys. Rev. C **78**, 037304 (2008).
[33] G. Audi, A. H. Wapstra, and C. Thibault, Nucl. Phys. A **729**, 337 (2003).
[34] T. Engeland, the OSLO shell-model code 1991–2006 (unpublished).
[35] K. A. Gridnev, D. K. Gridnev, V. G. Kartavenko, V. E. Mitroshin, V. N. Tarasov, D. V. Tarasov, and W. Greiner, Phys. At. Nucl. **69**, 1 (2006).
[36] L. Capelli, G. Colò, and J. Li, Phys. Rev. C **79**, 054329 (2009).
[37] T. Duguet and G. Hagen, Phys. Rev. C **85**, 034330 (2012).
[38] G. Hagen, M. Hjorth-Jensen, G. R. Jansen, R. Machleidt, and T. Papenbrock, Phys. Rev. Lett. **109**, 032502 (2012).
[39] L. Coraggio, A. Covello, A. Gargano, and N. Itaco, Phys. Rev. C **80**, 044311 (2009).
[40] D. Steppenbeck, S. Takeuchi, N. Aoi, P. Doornenbal, M. Matsushita, H. Wang, H. Baba, N. Fukuda, S. Go, M. Honma *et al*., Nature (London) **502**, 207 (2013).
[41] H. L. Crawford, R. M. Clark, P. Fallon, A. O. Macchiavelli, T. Baugher, D. Bazin, C. W. Beausang, J. S. Berryman, D. L. Bleuel, C. M. Campbell *et al*., Phys. Rev. Lett. **110**, 242701 (2013).
[42] P. T. Hosmer, H. Schatz, A. Aprahamian, O. Arndt, R. R. C. Clement, A. Estrade, K.-L. Kratz, S. N. Liddick, P. F. Mantica, W. F. Mueller *et al*., Phys. Rev. Lett. **94**, 112501 (2005).
[43] T. Marchi, G. de Angelis, T. Baugher, D. Bazin, J. Berryman, A. Bonaccorso, R. Clark, L. Coraggio, A. Covello, H. Crawford *et al*., EPJ Web Conf. **63**, 01021 (2013).
[44] N. Aoi, S. Kanno, S. Takeuchi, H. Suzuki, D. Bazin, M. D. Bowen, C. M. Campbell, J. M. Cook, D.-C. Dinca, A. Gade *et al*., Phys. Lett. B **692**, 302 (2010).
[45] N. Shimizu, T. Abe, Y. Tsunoda, Y. Utsuno, T. Yoshida, T. Mizusaki, M. Honma, and T. Otsuka, Prog. Theor. Exp. Phys. **2012**, 01A205 (2012).
[46] K. Kaneko, Y. Sun, M. Hasegawa, and T. Mizusaki, Phys. Rev. C **78**, 064312 (2008).
[47] A. Poves, E. Caurier, F. Nowacki, and K. Sieja, Phys. Scr. T **150**, 014030 (2012).
[48] H. Suzuki, N. Aoi, E. Takeshita, S. Takeuchi, S. Ota, H. Baba, S. Bishop, T. Fukui, Y. Hashimoto, E. Ideguchi *et al*., Phys. Rev. C **88**, 024326 (2013).
[49] Data extracted using the NNDC On-line Data Service from the XUNDL database, file revised as of September 12, 2013.